High Power Laser Science and Engineering, (2024), Vol. 12, e67, 8 pages.
doi:10.1017/hpl.2024.41

HIGH POWER LASER SCIENCE AND ENGINEERING

RESEARCH ARTICLE

A 7-kW narrow-linewidth fiber amplifier assisted by optimizing the refractive index of the large-mode-area active fiber

Pengfei Ma[1,2,3], Tianfu Yao[1,2,3], Wei Liu[1,2,3], Zhiyong Pan[1,2,3], Yisha Chen[1,2,3], Huan Yang[1,2,3], Zilun Chen[1,2,3], Zefeng Wang[1,2,3], Pu Zhou[1], and Jinbao Chen[1,2,3]

[1] *College of Advanced Interdisciplinary Studies, National University of Defense Technology, Changsha, China*

[2] *Nanhu Laser Laboratory, National University of Defense Technology, Changsha, China*

[3] *Hunan Provincial Key Laboratory of High Energy Laser Technology, National University of Defense Technology, Changsha, China*

(Received 10 April 2024; revised 4 July 2024; accepted 7 August 2024)

Abstract

The high-power narrow-linewidth fiber laser has become the most widely used high-power laser source nowadays. Further breakthroughs of the output power depend on comprehensive optimization of stimulated Brillouin scattering (SBS), stimulated Raman scattering (SRS) and transverse mode instability (TMI). In this work, we aim to further surpass the power record of all-fiberized and narrow-linewidth fiber amplifiers with near-diffraction-limited (NDL) beam quality. SBS is suppressed by white-noise-signal modulation of a single-frequency seed. In particular, the refractive index of the large-mode-area active fiber in the main amplifier is controlled and fabricated, which could simultaneously increase the effective mode field area of the fundamental mode and the loss coefficient of higher-order modes for balancing SRS and TMI. Subsequent experimental measurements demonstrate a 7.03 kW narrow-linewidth fiber laser with a signal-to-noise ratio of 31.4 dB and beam quality factors of $M_x^2 = 1.26$, $M_y^2 = 1.25$. To the best of our knowledge, this is the highest reported power with NDL beam quality based on a directly laser-diode-pumped and all-fiberized format, especially with narrow-linewidth spectral emission.

Keywords: fiber amplifier; fiber evaluation; high power; narrow linewidth

1. Introduction

The high-power fiber laser with near-diffraction-limited (NDL) beam quality is one of the research hotspots in the field of laser technology as a result of their relatively low cost, high output power, ease of maintenance, etc.[1–4]. A narrow-linewidth fiber amplifier based on a master oscillator power amplifier (MOPA) and all-fiberized format is the most versatile and efficient configuration for power scaling of a monolithic fiber source for spectral beam combining and coherent beam combining[5,6]. Previous studies have shown that the output power limits of NDL fiber amplifiers are set by the pump brightness, nonlinearity and thermal effect[7–11]. Thereinto, stimulated Raman scattering (SRS) and transverse mode instability (TMI) are proved to be the primary limitations in high-power NDL fiber amplifiers. As for narrow-linewidth spectral characteristics, stimulated Brillouin scattering (SBS) should also be carefully considered[12]. Up to now, over 10 kW power levels have been achieved by the tandem pumping format with broadband spectral emission[13,14]. In particular, as high as 6 kW power levels have been presented by direct pumping with a laser diode (LD) both in broadband and narrow-linewidth emissions by comprehensively balancing SRS, TMI and even SBS[15,16].

In principle, SBS and SRS thresholds are closely related to the total net gains of Raman and Brillouin Stokes lights[17–19]. In practical narrow-linewidth fiber amplifiers, SBS suppression commonly focuses on the construction of seed lasers for broadening the SBS gain spectrum, in which phase modulation of a single-frequency laser is the prevailing manner for simultaneously alleviating spectral broadening and

Correspondence to: J. Chen, College of Advanced Interdisciplinary Studies, National University of Defense Technology, No. 109 Deya Road, Changsha 410073, China. Email: kdchenjinbao@aliyun.com

maintaining temporal stability for the higher SRS threshold in the cascaded amplification process[20–23]. As for SRS suppression, a large effective mode field area (EMFA) of the fundamental mode (FM), a high pump absorption coefficient with short active fiber length and a counter-pumped manner could be adopted[7,8,11]. The TMI threshold is determined by many factors in the system design, such as the signal/pump wavelength, core/cladding diameters, core numerical aperture (NA) and pump power distribution. The effects of the aforementioned factors on the TMI threshold have been extensively studied, and different techniques for manipulating the thermally induced index grating and decreasing higher-order modes (HOMs) along the fiber have been validated[24,25]. All the same, coiling the active fiber to increase the relative losses of HOMs is among the few efficient strategies to enhance the TMI threshold above 5 kW narrow-linewidth systems[16,26–29]. Notably, the effect of this technique on TMI suppression will gradually alleviate along with the increase of core diameter and NA[30]. It is worth emphasizing that SRS and TMI are also interrelated in the design of high-power fiber amplifiers, and inter-contradictions exist for system design with respect to heat load, effective fiber length and core diameter[24,25,31–34]. More importantly, the TMI threshold in narrow-linewidth fiber amplifiers is lower than that in broadband ones as a result of the washout effect of the interfering grating from different frequency components[35,36]. Considering the multiple aspects above, further scaling the output power of LD-pumped narrow-linewidth all-fiberized fiber amplifiers becomes extremely challenging.

In this paper, a high-power all-fiberized and narrow-linewidth fiber amplifier with NDL beam quality assisted by optimizing the refractive index of the large-mode-area (LMA) active fiber is presented. By sinking the central area and controlling the NA of active fiber, SRS and TMI are well balanced by increasing the EMFA of FM and the loss coefficient of HOMs with the help of bending-loss technology. Record output power of a 7.03 kW narrow-linewidth fiber laser is demonstrated with a signal-to-noise ratio (SNR) of 31.4 dB and beam quality factors of $M_x^2 = 1.26$, $M_y^2 = 1.25$. To the best of our knowledge, the power level achieved is not only the highest of any narrow-linewidth fiber laser, but also a new record for LD-pumped all-fiberized fiber amplifiers with NDL beam quality.

2. Experimental setup

Experimental setup of the all-fiberized fiber amplifier is schematically shown in Figure 1. It is a typical fiber amplifier based on a MOPA configuration. The master oscillator (MO) is a low-noise single-frequency fiber laser based on an ultra-cavity[37]. The central wavelength and output power are measured to be 1080 nm and 50 mW, respectively. In order to suppress SBS, external phase modulation with white-noise-signal (WNS) modulation is performed based on a $LiNbO_3$ electro-optic modulator (EOM). The insertion loss of the EOM is about 3 dB, and the delivered fiber laser is injected into cascaded fiber amplifiers for further power scaling. A commercial pre-amplification module (PAM, from Precilasers) is employed to scale the output power to approximately 30 W. An optical circulator (OC) embedded with band-pass filtering with a transmission bandwidth of 3 nm is fused in the rear end of the PAM for simultaneously filtering the background spectral noise and monitoring and exporting the backward power from the main fiber amplifier. A mode field adaptor (MFA) is used to match the laser delivery from the output port of the OC to the main fiber amplifier.

The main amplifier is bidirectionally pumped by 12 wavelength stabilized LDs at 976 nm, and is coupled into the large-mode-area Yb-doped active fiber (LMA-YDF) by two fiberized (6 + 1) × 1 signal-pump combiners. The maximum available pump power of each LD is 0.87 kW. The core/cladding diameters of the delivery fibers are 20/250 and 20/400 μm with NA ~ 0.063 for the forward signal-pump

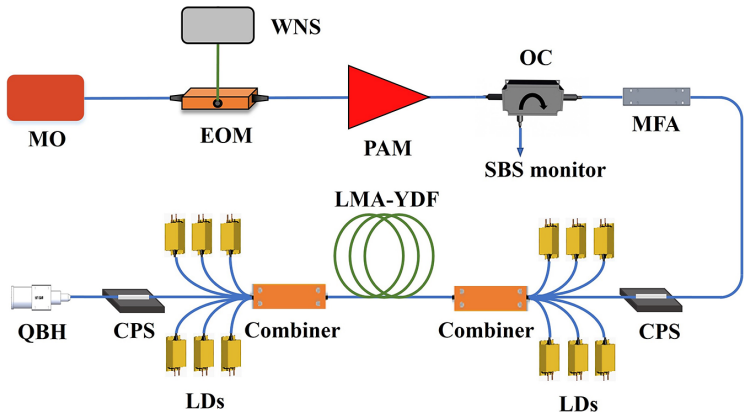

Figure 1. Experimental setup of the all-fiberized fiber amplifier.

https://doi.org/10.1017/hpl.2024.41 Published online by Cambridge University Press

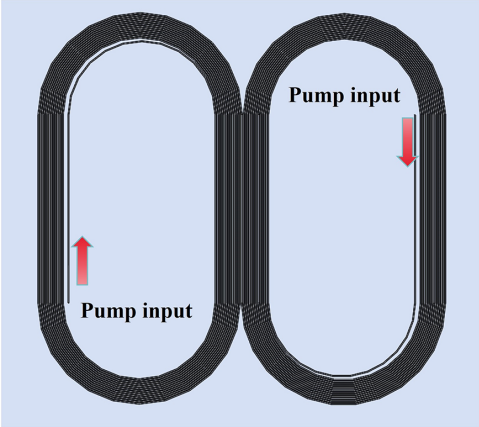

Figure 2. Schematic of the assembled active fiber.

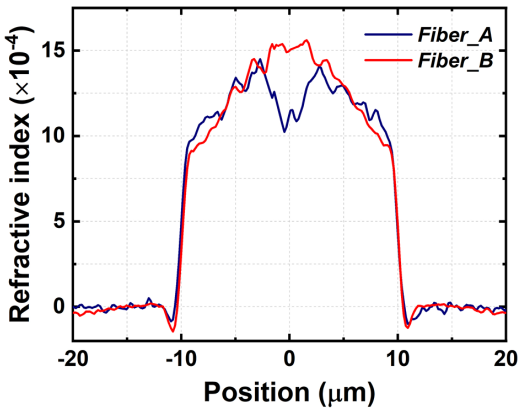

Figure 3. Measured refractive index profiles for the two YDFs.

combiner, and the core/cladding diameters of the delivery fibers are 25/400 and 25/250 μm with NA ~ 0.065 for the backward one. Two cladding power strippers (CPSs) based on corrosion technology are spliced to remove the residual pump and cladding signal light. A quartz block holder (QBH) is terminated to deliver the fiber laser into free space. The overall length of the transmission fiber after the Yb-doped active fiber (YDF) is about 1.8 m in the experiment.

The YDF employed in the main amplifier is a 14 m home-made LMA-YDF with uniform core/cladding diameters of 20/400 μm, which is fabricated by the modified chemical vapor deposition (MCVD) method. The core NA and absorption coefficient are measured to be 0.059 and 1.2 dB/m at 976 nm, respectively. As for the design of the YDF bending and cooling plate structure, a symmetrical double runway active water cooling board is employed in the experiment for incorporating bending loss for TMI suppression. The inner circle radii are set to be 40 mm, and the spacing of two adjacent circles is 1 mm, as shown in Figure 2. The seeding laser is injected from the inner circle of the main amplifier to increase the relative loss of the higher-order-mode within the regions with large thermal gradient, consequently fulfilling TMI suppression[30].

3. Refractive index optimization of large-mode-area active fiber

Various fiber parameters could simultaneously change the TMI and SRS thresholds of high-power fiber amplifiers, such as the core/cladding diameter, core NA, ratio of the doping area, cladding pump absorption coefficient or effective fiber length. For most of the factors above, SRS and TMI thresholds are inter-contradicted in the design of high-power fiber amplifiers[24,25,31–34]. Notably, a decrease in NA could increase the EMFA of FM, and the SRS threshold of a fiber amplifier could be correspondingly enhanced for NDL operation[17]. Besides, the decrease of NA could increase the relative losses of HOMs in a specific coiling manner, which also has the advantage of TMI suppression[30,38].

In general, the EMFA of FM and the loss characteristics have been widely estimated by using the core diameter, NA and coiling radius of the active fiber[39]. However, the core NA is typically an averaged approximate value for the cross-sectional refractive index profile (RIP), with which it is difficult to estimate the perturbations of the RIP accurately. Consequently, optimization of the active fiber in this work is performed on the control of cross-sectional RIP. Figure 3 illustrates the measured RIP of this home-made YDF (Fiber_A), and the RIP of YDF (Fiber_B) employed in our previous reported 6.12 kW narrow-linewidth fiber amplifier is also given for comparison[16]. A peak–valley (PV) value of approximately 4×10^{-4} and bottom side of approximately 5.5 μm within an inverted triangle have tentatively been generated. The incorporation of a sinking area will sacrifice the EMFA of FM to some extent, but the bending loss increases significantly for TMI suppression. Further, the fall of the EMFA of FM could be compensated by decreasing the average core NA. Compared with the RIP of Fiber_B, the average core NA of Fiber_A is decreased from 0.061 to 0.059. Overall, the EMFA of FM and bending loss of HOMs could increase simultaneously (as shown below), which is beneficial for achieving higher output power in a fiber amplifier by better comprehensive balancing of SRS and TMI.

The EMFA of FM for the two YDFs under different coiling radii is calculated based on the finite element method by using the measured RIP shown in Figure 2, which is depicted in Figure 4(a). As shown in Figure 4(a), variation of the EMFA for a specific YDF is slight when the coiling radius is different. The EMFA of Fiber_A is 12.4% larger than that of Fiber_B in different cases. Based on the EMFA of FM for the two YDFs, we could simulate the enhancement ratio of the SRS threshold for this fiber amplifier employing Fiber_A compared to the fiber amplifier employing Fiber_B through the conventional SRS model[19]. Figure 4(b) illustrates the

https://doi.org/10.1017/hpl.2024.41 Published online by Cambridge University Press

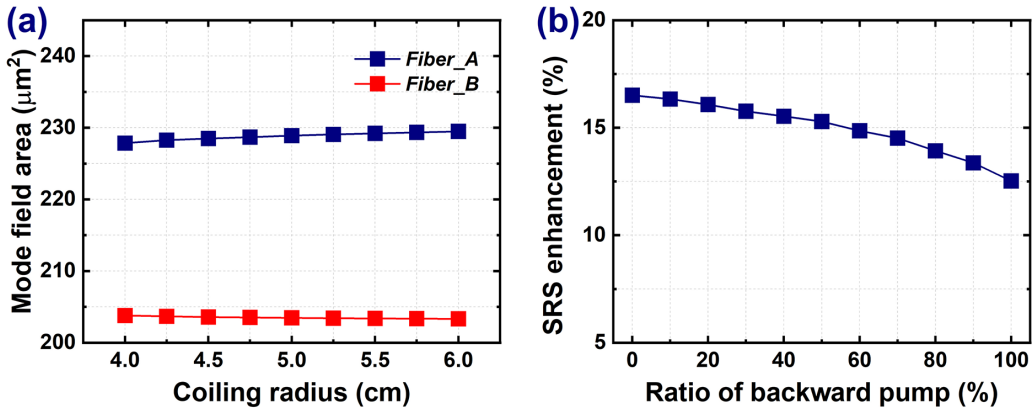

Figure 4. (a) EMFAs of FM for the two YDFs under different coiling radii. (b) SRS enhancement when the power ratio of the backward pump is different.

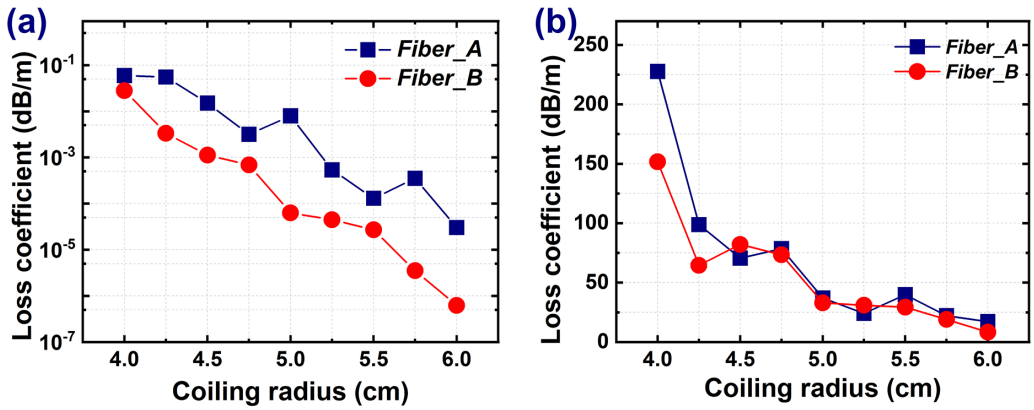

Figure 5. Loss coefficient of transverse modes for the two YDFs under different coiling radii: (a) LP_{01} mode, (b) LP_{11} mode.

corresponding SRS enhancement when the power ratio of the backward pump is different. As shown in Figure 4(b), SRS enhancement decreases as a function of the backward pump ratio, while SRS enhancement is over 12.5% at different backward pump ratios.

The loss coefficients of the LP_{01} and LP_{11} modes for the two YDFs under different coiling radii are shown in Figures 5(a) and 5(b), respectively. As shown in Figure 5, the overall loss coefficients of the LP_{01} and LP_{11} modes for a specific YDF decrease as a function of the coiling radius. From Figure 5(a), it is shown that the loss coefficient of the LP_{01} mode for Fiber_A is always higher than that for Fiber_B under the same coiling radius, and the loss coefficients of LP_{01} are calculated to be 0.059 and 0.026 dB/m for Fiber_A and Fiber_B, respectively, when the coiling radius is set to 4 cm. As shown in Figure 5(b), the loss coefficient of the LP_{11} mode for Fiber_A is comparable to that of Fiber_B when the coiling radius ranges from 4.5 to 6.0 cm. Notably, the loss coefficient of the LP_{11} mode for Fiber_A is larger than that of Fiber_B when the coiling radius is smaller than 4.25 cm. When the coiling radius is set to 4 cm, the loss coefficient of the LP_{11} mode for Fiber_A is 227.7 dB/m, which is 1.5 times larger than that of Fiber_B (151.6 dB/m).

4. Experimental results

Firstly, the spectra of the modulated MO and those after the PAM are characterized, which are shown in Figure 6. From the results in Figure 6, the spectral distributions and linewidths are maintained well in the pre-amplification process. After the PAM, the 3 dB linewidth is measured to be 0.83 nm.

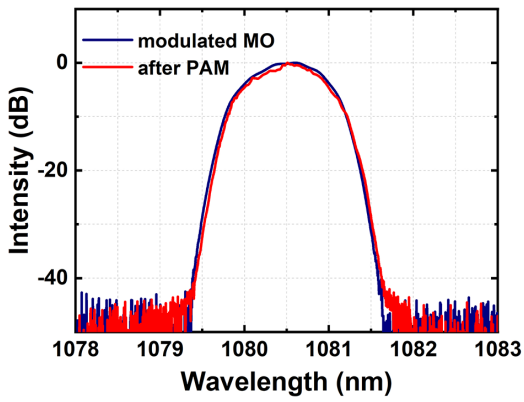

Figure 6. Measured spectra of the modulated MO and after the PAM.

https://doi.org/10.1017/hpl.2024.41 Published online by Cambridge University Press

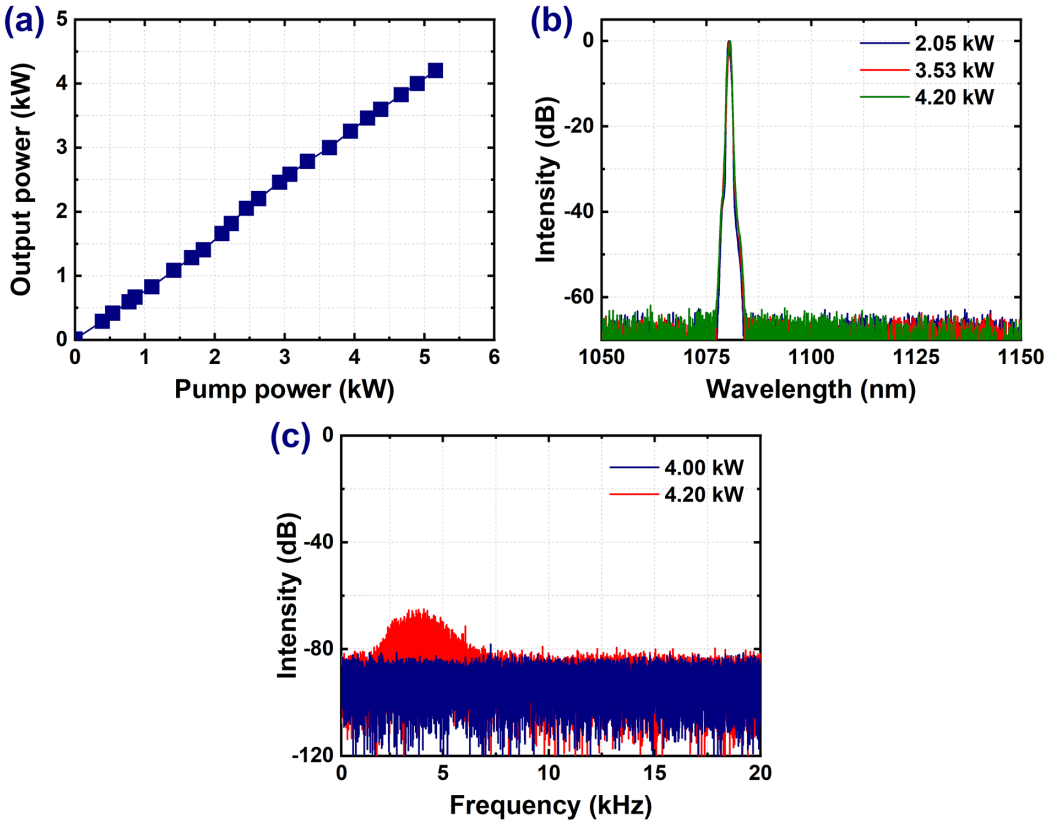

Figure 7. Output properties of the fiber amplifier with backward pumping: (a) power curve; (b) typical spectra; (c) Fourier transformation of the temporal trace.

Then, the characteristics of the narrow-linewidth fiber amplifier with backward pumping are investigated, and the output power conversion with pump power is shown in Figure 7(a). The slope efficiency is fitted to be 83.3%, and the output power of 4.20 kW is achieved at the pump power of 5.16 kW with an optical-to-optical conversion efficiency of 81.5%. The output spectra at several typical output powers are shown in Figure 7(b). At the maximum output power, the 3 dB spectral linewidth is measured to be 0.41 nm. In the experiment, when increasing the backward pump power from 4.90 kW (signal power of 4.00 kW) to 5.16 kW (signal power of 4.20 kW), a noise-like envelope is observed in the Fourier transformation of the temporal trace within 5 kHz, which is shown in Figure 7(c). Thus, TMI occurs at the pump power of 5.16 kW for the narrow-linewidth fiber amplifier with backward pumping.

Similarly, the output power, spectrum and Fourier transformation of the temporal trace for the narrow-linewidth fiber amplifier with forward pumping are also examined, and the typical results are listed in Figures 8(a)–8(c). As shown in Figure 8(a), when the pump power is 4.23 kW, the output power increases linearly to 2.69 kW with a slope efficiency of 63.9%. There is a power stagflation to 2.70 kW when further increasing the pump power to 4.38 kW. At the pump power of 4.23 kW, the optical-to-optical conversion efficiency is 63.7% and the 3 dB spectral linewidth is measured to be 0.75 nm (shown in Figure 8(b)). As shown in Figure 8(c), a TMI-induced Fourier envelope within 5 kHz emerges. By comparison between the power conversions of the backward and forward cases, it is inferred that an obvious discrepancy of conversion efficiency exists in the experiment. This phenomenon might be attributed to the difference of power distribution with forward and backward pumps, because the overall loss induced by the bending active fiber is an integrated effect of the power distribution and the loss coefficient.

Figure 9(a) illustrates the output power of this fiber amplifier in the bidirectional pumping scheme. In this case, we firstly increase the forward pump power to scale the output power to 1.01 kW, then increase the backward pump power to scale the output power to 5.35 kW, and finally increase the forward pump power to 7.03 kW. As shown in Figure 9(a), the output power of the signal laser increases almost linearly with the pump power. The maximum output power is 7.03 kW at the pump power of 9.4 kW with an overall conversion efficiency of 74.2%. The corresponding forward and backward pump powers are 4.23 and 5.16 kW, respectively. An interesting phenomenon is observed in that the ultimate output power of bidirectional pumping is a little beyond the total power of sole backward and forward pumping at 4.23 and 5.16 kW, respectively. This result may be attributed to the fact that the temperature increase

https://doi.org/10.1017/hpl.2024.41 Published online by Cambridge University Press

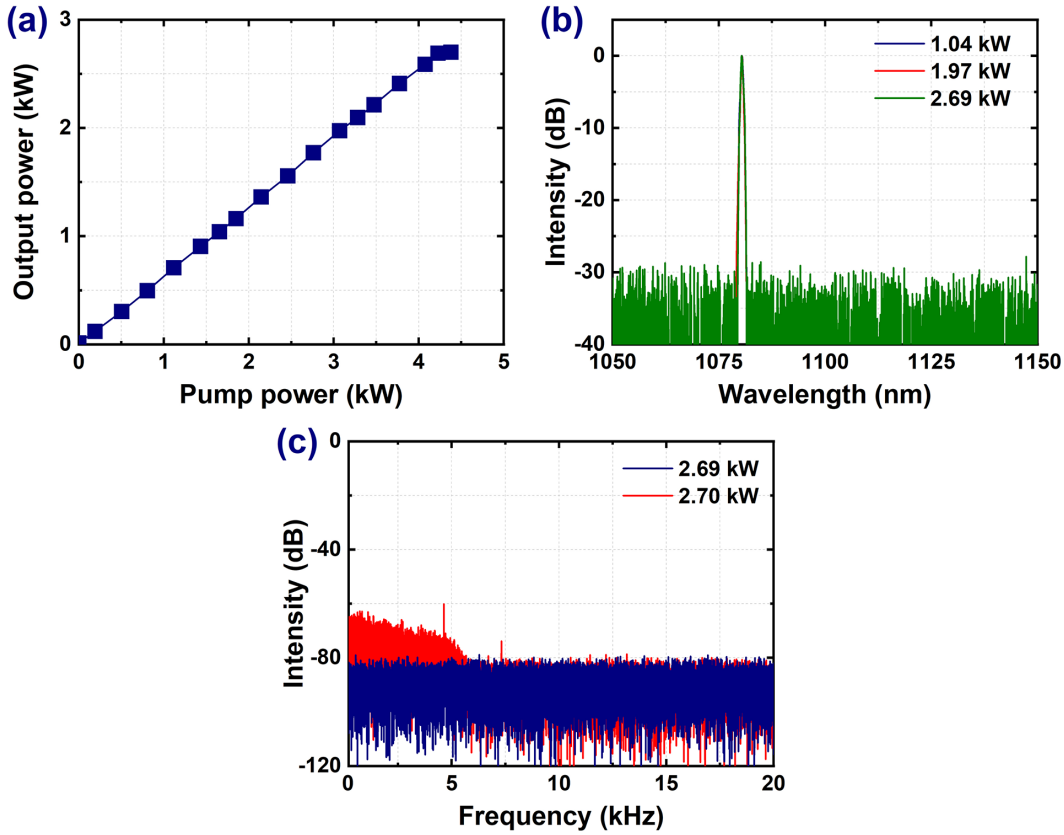

Figure 8. Output properties of the fiber amplifier with forward pumping: (a) power curve; (b) typical spectra; (c) Fourier transformation of the temporal trace.

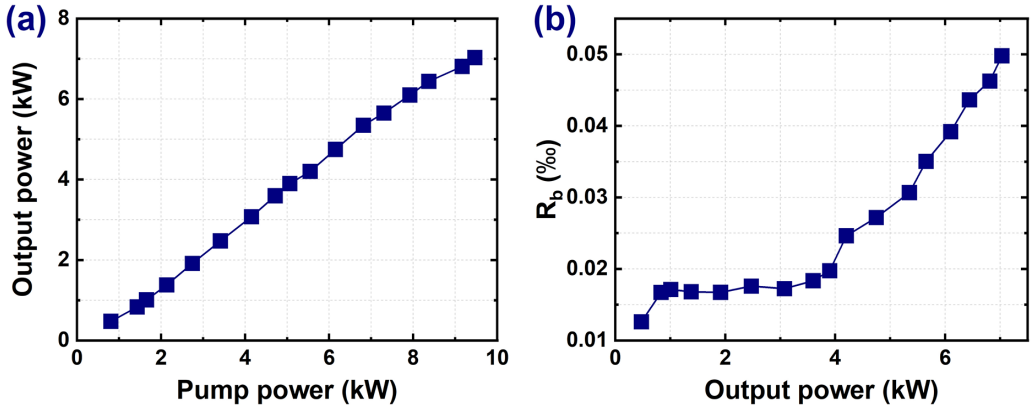

Figure 9. (a) Output power of the signal laser at different pump powers with bidirectional pumping; (b) backward power ratio (R_b) at different output powers.

at the backward end of the fiber enlarges the core NA and decreases the transmission loss induced by bending for the forward signal with bidirectional pumping[39,40]. In our experiment, backward power collected by the OC is measured to monitor the SBS effect. The evolution of the backward power ratio (R_b) along with output power is shown in Figure 9(b), in which R_b is defined as the ratio of backward power and the output power. In general, the increased slope of R_b for forward pumping is greater than that for backward cases. Specifically, when the output power is increased from 1.01 kW to 5.35 kW power level by backward pumping, R_b changes from 0.017‰ to 0.031‰. When forward pump power is injected, R_b is increased near linearly along with power scaling. At maximal output power, R_b is calculated to be within 0.05‰. In the whole amplification process, an exponential nonlinear growth trend is not observed, which reveals that the fiber amplifier is operated below the SBS threshold.

Figure 10(a) illustrates the output spectra of the signal laser at different output powers. As shown in Figure 10(a),

https://doi.org/10.1017/hpl.2024.41 Published online by Cambridge University Press

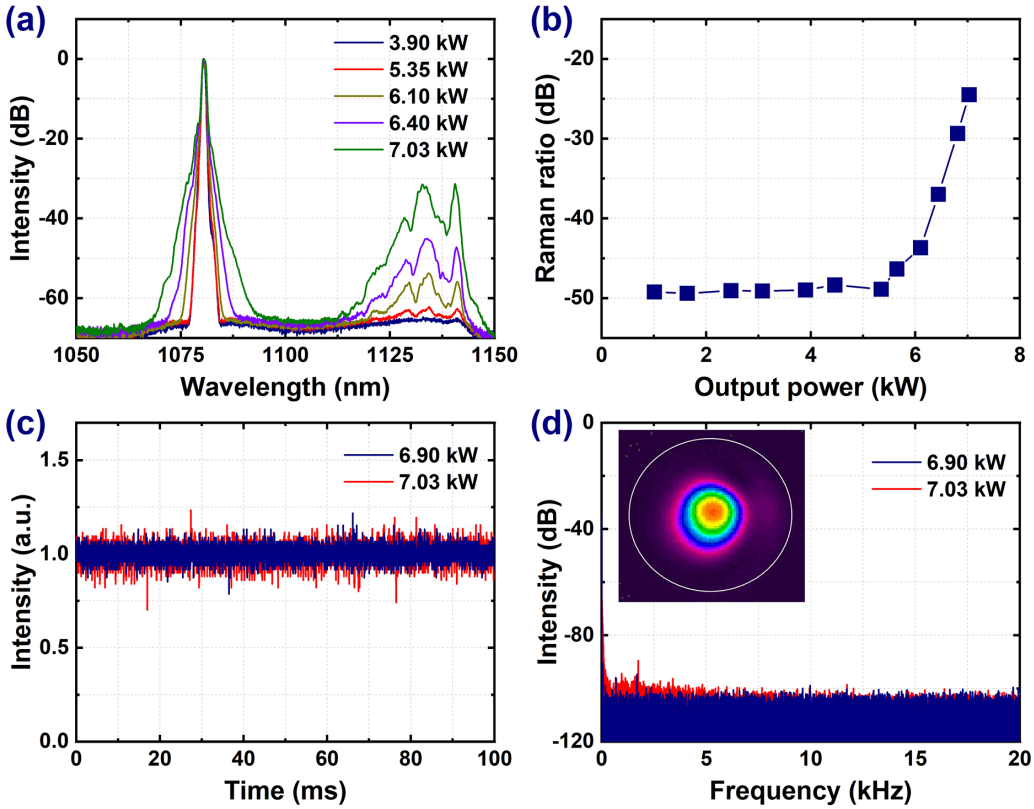

Figure 10. Output properties of the fiber amplifier with bidirectional pumping: (a) typical spectra; (b) Raman ratio; (c) temporal trace; (d) Fourier transformation (inset: the beam profile at focal length of M2-200s).

the spectral wing broadens along with the enhancement of SRS. This phenomenon could be understood through the four-wave-mixing induced spectral wing broadening[23]. The 3 and 20 dB spectral linewidths of the signal laser are 0.76 and 2.92 nm at the maximum output power, respectively. The spectral component near 1135 nm begins to increase at the output power of 5.35 kW. The peak SNR is 31.4 dB compared with the Raman Stokes light at the maximum output power. The corresponding power ratio of Raman Stokes light (defined by the Raman ratio) is calculated through dividing the integrated spectrum from 1110 to 1150 nm by the integrated spectrum from 1050 to 1150 nm from the spectra, which is shown in Figure 10(b). It is illustrated that the Raman ratio remains around –49.0 dB when the output power is below 5.35 kW, grows slightly to –43.7 dB at the output power of 6.10 kW, and quickly reaches –24.5 dB (0.36%) at the maximum output power. The normalized temporal trace and the corresponding Fourier transformation of the signal laser at different output powers are demonstrated in Figures 10(c) and 10(d). The intensity fluctuation and frequency envelope show an increasing trend, which reveals that the narrow-linewidth fiber amplifier also operates near the TMI threshold. At the maximum output power, the beam quality (M^2 factor) of signal laser is measured by using M2-200s, and the M^2 factors in the x/y directions are $M_x^2 = 1.26$ and $M_y^2 = 1.25$, respectively. The inset in Figure 10(d) is the beam profile at a focal length of M2-200s, which also shows that NDL beam quality has been achieved.

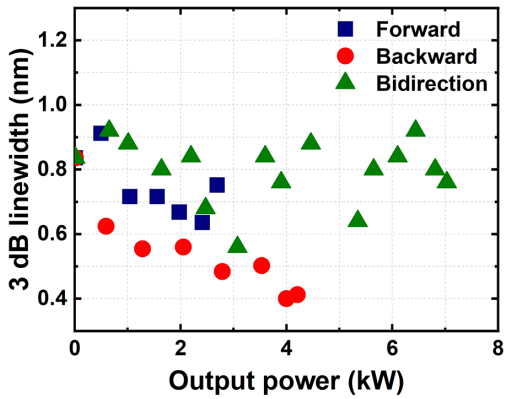

Figure 11. Measured 3 dB spectral linewidth for different output powers and pump processes.

The measured 3 dB spectral linewidth of the signal laser at different output powers and pumping processes is shown in Figure 11. As shown in Figure 11, the overall spectral linewidth of 3 dB is related to the output power, pump power direction and forward/backward pump power ratio, which is unstable along with power scaling. The phenomena shown in Figure 11 are possibly because the intensity noise fluctuation induced by the phase-modulated process could

https://doi.org/10.1017/hpl.2024.41 Published online by Cambridge University Press

produce frequency chirp through the self-phase modulation effect[41–43], which will enhance or weaken the original phase modulation at different output powers and ultimately induce the change of the 3 dB spectral linewidth.

5. Conclusion

In this work, we demonstrate a record 7-kW all-fiberized and narrow-linewidth fiber amplifier with NDL beam quality. The impact of SBS is suppressed by WNS modulation of a single-frequency seed, and SRS and TMI are well balanced by optimizing the refractive index of LMA active fiber. The advantages of optimized active LMA fiber for simultaneous increase of the EMFA of FM and the loss coefficient of HOMs are quantitatively analyzed. The power scaling ability and spectral and temporal characteristics of forward and backward pump processes are respectively investigated. Further, a 7.03 kW narrow-linewidth fiber laser with an SNR of 31.4 dB and beam quality factors of $M_x^2 = 1.26$, $M_y^2 = 1.25$ is fulfilled by bidirectional pumping. We believe that this work could provide new insights and design strategies for higher-power narrow-linewidth fiber lasers with NDL beam quality.

Acknowledgement

This work was supported by the National Key Research and Development Program of China (No. 2022YFB3606400) and the National Natural Science Foundation of China (No. U22A6003).

References

1. D. J. Richardson, J. Nilsson, and W. A. Clarkson, J. Opt. Soc. Am. B **27**, B63 (2010).
2. W. Shi, Q. Fang, X. Zhu, R. A. Norwood, and N. Peyghambarian, Appl. Opt. **53**, 6554 (2014).
3. M. N. Zervas and C. A. Codemard, IEEE J. Sel. Top. Quantum Electron. **20**, 219 (2014).
4. J. Zuo and X. Lin, Laser Photon. Rev. **16**, 2100741 (2022).
5. Y. Zheng, Y. Yang, J. Wang, M. Hu, G. Liu, X. Zhao, X. Chen, K. Liu, C. Zhao, B. He, and J. Zhou, Opt. Express **24**, 12063 (2016).
6. Z. Liu, P. Ma, R. Su, R. Tao, Y. Ma, X. Wang, and P. Zhou, J. Opt. Soc. Am. B **34**, A7 (2017).
7. J. W. Dawson, M. J. Messerly, R. J. Beach, M. Y. Shverdin, E. A. Stappaerts, A. K. Sridharan, P. H. Pax, J. E. Heebner, C. W. Siders, and C. P. J. Barty, Opt. Express **16**, 13240 (2008).
8. H. Otto, C. Jauregui, J. Limpert, and A. Tünnermann, Proc. SPIE **9728**, 97280E (2016).
9. M. N. Zervas, Opt. Express **27**, 19019 (2019).
10. L. Dong, J. Ballato, and J. Kolis, Opt. Express **31**, 6690 (2023).
11. Y. Wang, Opt. Eng. **44**, 114202 (2005).
12. A. Kobyakov, M. Sauer, and D. Chowdhury, Adv. Opt. Photon. **2**, 1 (2010).
13. IPG Photonics Corporation, "IPG Photonics successfully tests world's first 10 kilowatt single-mode production laser," http://www.ipgphotonics.com (2009).
14. B. Shiner, "The impact of fiber laser technology on the world wide material processing market," in *CLEO: Applications and Technology* (2013), paper AF2J.1.
15. B. Yang, P. Wang, H. Zhang, X. Xi, C. Shi, X. Wang, and X. Xu, Opt. Express **29**, 26366 (2021).
16. G. Wang, J. Song, Y. Chen, S. Ren, P. Ma, W. Liu, T. Yao, and P. Zhou, High Power Laser Sci. Eng. **10**, e22 (2022).
17. R. G. Smith, Appl. Opt. **11**, 2489 (1972).
18. J. Wang, D. Yan, S. Xiong, B. Huang, and C. Li, Opt. Express **24**, 14463 (2016).
19. W. Liu, P. Ma, H. Lv, J. Xu, P. Zhou, and Z. Jiang, Opt. Express **24**, 26715 (2016).
20. A. Flores, C. Robin, A. Lanari, and I. Dajani, Opt. Express **22**, 17735 (2014).
21. C. Yu, O. Shatrovoy, T. Fan, and T. Taunay, Opt. Lett. **41**, 5202 (2016).
22. F. Beier, C. Hupel, S. Kuhn, S. Hein, J. Nold, F. Proske, B. Sattler, A. Liem, C. Jauregui, J. Limpert, N. Haarlammert, T. Schreiber, R. Eberhardt, and A. Tunnermann, Opt. Express **25**, 14892 (2017).
23. W. Liu, J. Song, P. Ma, H. Xiao, and P. Zhou, Photon. Res. **9**, 424 (2021).
24. R. Tao, X. Wang, and P. Zhou, IEEE J. Sel. Top. Quantum Electron. **24**, 0903319 (2018).
25. C. Jauregui, C. Stihler, and J. Limpert, Adv. Opt. Photon. **12**, 429 (2020).
26. P. Ma, H. Xiao, W. Liu, H. Zhang, X. Wang, J. Leng, and P. Zhou, High Power Laser Sci. Eng. **9**, e45 (2021).
27. Z. Huang, Q. Shu, R. Tao, Q. Chu, Y. Luo, D. Yan, X. Feng, Y. Liu, W. Wu, H. Zhang, H. Lin, J. Wang, and F. Jing, IEEE Photon. Technol. Lett. **33**, 1181 (2021).
28. Y. Wang, W. Peng, H. Liu, X. Yang, H. Yu, Y. Wang, J. Wang, Y. Feng, Y. Sun, Y. Ma, Q. Gao, and C. Tang, Opt. Lett. **48**, 2909 (2023).
29. S. Liao, T. Luo, R. Xiao, C. Shu, J. Cheng, Z. Zhang, Y. Xing, H. Li, N. Dai, and J. Li, Opt. Lett. **48**, 6533 (2023).
30. R. Tao, R. Su, P. Ma, X. Wang, and P. Zhou, Laser Phys. Lett. **14**, 025101 (2017).
31. K. Hejaz, M. Shayganmanesh, R. Rezaei-Nasirabad, A. Roohforouz, S. Azizi, A. Abedinajafi, and V. Vatani, Opt. Lett. **42**, 5274 (2017).
32. W. Liu, P. Ma, C. Shi, P. Zhou, and Z. Jiang, Opt. Express **26**, 15793 (2018).
33. C. Zhang, R. Tao, M. Li, X. Feng, R. Liao, Q. Chu, L. Xie, H. Li, B. Shen, L. Xu, and J. Wang, J. Lightwave Technol. **41**, 671 (2023).
34. V. Distler, F. Möller, M. Strecker, G. Palma-Vega, T. Walbaum, and T. Schreiber, Opt. Express **28**, 22819 (2020).
35. J. J. Smith and A. V. Smith, Proc. SPIE **9344**, 93440L (2015).
36. S. Ren, W. Lai, G. Wang, W. Li, J. Song, Y. Chen, P. Ma, W. Liu, and P. Zhou, Opt. Express **30**, 7845 (2022).
37. Y. Sun, Q. Zhao, C. Wang, C. Zeng, W. Lin, C. Yang, Z. Feng, Q. Zhang, Z. Yang, and S. Xu, Opt. Lett. **47**, 4475 (2022).
38. R. Tao, P. Ma, X. Wang, P. Zhou, and Z. Liu, Laser Phys. Lett. **12**, 085101 (2015).
39. R. T. Schermer and J. H. Cole, IEEE J. Quantum Electron. **43**, 899 (2007).
40. D. C. Brown and H. J. Hoffman, IEEE J. Quantum Electron. **37**, 207 (2001).
41. W. Liu, P. Ma, W. Lai, J. Song, S. Zhang, C. Li, H. Xiao, and P. Zhou, J. Lightwave Technol. **39**, 6413 (2021).
42. G. D. Goodno and J. E. Rothenberg, Opt. Express **27**, 13129 (2019).
43. H. Liu, Y. Feng, Y. Wang, Y. Wang, T. Li, S. Liu, X. Shi, J. Wei, Z. Yan, W. Peng, Y. Sun, J. Shang, Y. Ma, Q. Gao, and C. Tang, Opt. Express **31**, 28089 (2023).

https://doi.org/10.1017/hpl.2024.41 Published online by Cambridge University Press